International Journal of Mining Science and Technology xxx (xxxx) xxx

Contents lists available at ScienceDirect

International Journal of Mining Science and Technology

journal homepage: www.elsevier.com/locate/ijmst

Correlations between mineral composition and mechanical properties of granite using digital image processing and discrete element method

Changdi He [a,*], Brijes Mishra [a], Qingwen Shi [b], Yun Zhao [c], Dajun Lin [d], Xiao Wang [e,*]

[a] Department of Mining Engineering, University of Utah, Salt Lake City 84112, USA
[b] College of Mine Safety, North China Institute of Science and Technology, Langfang 065201, China
[c] Department of Mining Engineering, West Virginia University, Morgantown 26506, USA
[d] Department of Electrical and Computer Engineering, University of Utah, Salt Lake City 84112, USA
[e] College of Energy and Mining Engineering, Shandong University of Science and Technology, Qingdao 266590, China

ARTICLE INFO

Article history:
Received 11 October 2022
Received in revised form 13 May 2023
Accepted 24 June 2023
Available online xxxx

Keywords:
Granite
Digital image processing
Discrete element method
Mineral composition
Mechanical properties

ABSTRACT

This study investigated the correlations between mechanical properties and mineralogy of granite using the digital image processing (DIP) and discrete element method (DEM). The results showed that the X-ray diffraction (XRD)-based DIP method effectively analyzed the mineral composition contents and spatial distributions of granite. During the particle flow code (PFC2D) model calibration phase, the numerical simulation exhibited that the uniaxial compressive strength (UCS) value, elastic modulus (E), and failure pattern of the granite specimen in the UCS test were comparable to the experiment. By establishing 351 sets of numerical models and exploring the impacts of mineral composition on the mechanical properties of granite, it indicated that there was no negative correlation between quartz and feldspar for UCS, tensile strength (σ_t), and E. In contrast, mica had a significant negative correlation for UCS, σ_t, and E. The presence of quartz increased the brittleness of granite, whereas the presence of mica and feldspar increased its ductility in UCS and direct tensile strength (DTS) tests. Varying contents of major mineral compositions in granite showed minor influence on the number of cracks in both UCS and DTS tests.
© 2023 Published by Elsevier B.V. on behalf of China University of Mining & Technology This is an open access article under the CC BY-NC-ND license (http://creativecommons.org/licenses/by-nc-nd/4.0/).

1. Introduction

Many industries widely use granite as a host rock, including in radioactive waste storage, deep mining, enhanced geothermal systems (EGS), etc. [1]. The physicomechanical properties, such as UCS, tensile strength (σ_t), and elastic modulus (E), are three indices typically employed to represent the mechanical properties of a material [2]. Numerous researchers have used experimental, machine learning, and numerical methods to evaluate the mechanical properties of granite. Previous research has shown that the characteristics of granite, such as mineral compositions, mineral size distributions, mineral shapes, and micro defects, are correlated with their mechanical properties [3].

Du et al. [2] investigated the relationship between mechanical strength and grain size using UCS, Brazilian tension tests, and acoustic emission (AE). Their results showed that the strength of igneous rock was inversely proportional to the size of the mineral grains. Coggan et al. [4] used scanning electron microscopy (SEM), AE, and XRD to establish the relationship between the UCS and various alteration grades of granite samples. The recrystallization of minerals at boundaries can impact the strength of granite significantly. In addition, previous studies have found the texture of granite significantly impacts its strength variance, even with comparable alteration grades [5]. Yılmaz et al. [6] suggested that the spatial distribution of biotite mainly governed the Brazilian tensile strength of granite. The application of the split Hopkinson pressure bar (SHPB) and ultrasonic pulse transmission methods enabled the investigation of damage to granite rock caused by dynamic loadings [7]. However, the influence of mineral compositions on the mechanical properties of granite is not evident. For instance, Tuğrul and Zarif [8] demonstrated a positive linear relationship between the quartz-to-feldspar ratio and UCS for granite specimens. Nevertheless, in direct contrast to the experiments conducted on granitic rocks from Turkey [8], Sajid et al. [5] demonstrated a negative association between quartz contents and UCS.

Using multiple machine models can aid in establishing the relationship between the mineral contents of granite and their mechanical properties. Yesiloglu-Gultekin et al. [9] employed an adaptive neuro-fuzzy inference system (ANFIS) to discover the positive relationship between quartz and UCS. In contrast, the relationships between orthoclase and UCS, and plagioclase and UCS

* Corresponding authors.
E-mail addresses: changdi.he@utah.edu (C. He), x.wang@sdust.edu.cn (X. Wang).

https://doi.org/10.1016/j.ijmst.2023.06.003
2095-2686/© 2023 Published by Elsevier B.V. on behalf of China University of Mining & Technology
This is an open access article under the CC BY-NC-ND license (http://creativecommons.org/licenses/by-nc-nd/4.0/).

Please cite this article as: C. He, B. Mishra, Q. Shi et al., Correlations between mineral composition and mechanical properties of granite using digital image processing and discrete element method, International Journal of Mining Science and Technology, https://doi.org/10.1016/j.ijmst.2023.06.003

were negative. In addition, Sun et al. [10] analyzed the UCS of the jet-grouted coal-grout composite through gradient boosted regression tree (GBRT) and random forest (RF).

Several researchers have used the grain-based element model (GBM) to understand the effect of mineralogy, mineral properties, mineral boundary properties [11], and mineral size [12,13] on the tensile and compressive strength, fracture pattern, and development of specific crack types of granite [3]. During compression testing, Hu et al. [14] identified that mineral size, distribution, and grain boundary strength (normal strength, cohesion, and friction angle) were the most influential parameters on crack development in a rock specimen. They assigned four micro-parameters, i.e., particle modulus, parallel bond modulus, parallel bond tension strength, and parallel bond cohesion, to the Weibull distribution to reflect the micro-heterogeneity of rock. The analysis revealed that increasing heterogeneity leads to lower UCS, *E*, and a more dispersed distribution of microcrack inclination [14]. As the percentage of quartz increased, the mechanical strength, *E*, and the total number of microcracks increased. However, Poisson's ratio and maximum volumetric strain decreased gradually. The position of the mineral has a minor but insignificant effect on the simulated strength characteristics and micro-cracking behaviors [15]. To examine the dynamic fracture toughness and micro-cracking characteristics of granite at the grain scale, researchers developed the SHPB system through the Particle Flow Code 3D-grain-based element model (PFC3D-GBM) approach [16]. However, the studies mentioned above were generally limited to a narrow range of mineral component proportions in granite, and systematic investigations of the effects of mineral composition on mechanical properties were lacking.

The objective of this study is to comprehensively examine the mechanical properties of granites, which exhibit diverse material compositions, through the implementation of the DEM. Initially, this study conducted a literature review to analyze the impact of distinct mineral compositions on the mechanical characteristics of granite in experimental studies. In the subsequent stages of this investigation, data encompassing the mineralogical composition and spatial distribution in the granite sample were acquired through the application of the DIP technique. This gathered information was then imported into the PFC2D, facilitating the construction of an accurate model. The resulting PFC2D model properly replicated both the mineralogical content and spatial distribution pattern characteristic of the actual granite specimen. This PFC2D model was used to calibrate the parameters in comparison to experimental data. Afterward, developing 351 sets of PFC2D models with varying mineral compositions to explore an array of correlations, including the contents of quartz, feldspar, and mica to UCS, UCS failure strain (ε_{fail_UCS}), σ_t, DTS failure strain (ε_{fail_DTS}), the number of cracks in UCS (N_{crack_UCS}) and DTS (N_{crack_DTS}) tests, as well as *E*. Ultimately, this research compared the results procured from the discrete element methodology with findings from existing literature to ascertain the relationship between mechanical properties and mineral compositions of granite.

2. Literature review

2.1. Typical mineral compositions and properties of granite

Granite is a widespread rock type in the continental crust, primarily consisting of quartz (10% to 50%), potassium feldspar (K-feldspar), and sodium feldspar (plagioclase). These minerals comprise more than 80% of the compositions of granite, with other common minerals including mica (muscovite and biotite) and amphibole [17]. Fig. 1a is the phase diagram for the feldspar system, which represents the relationships between the different

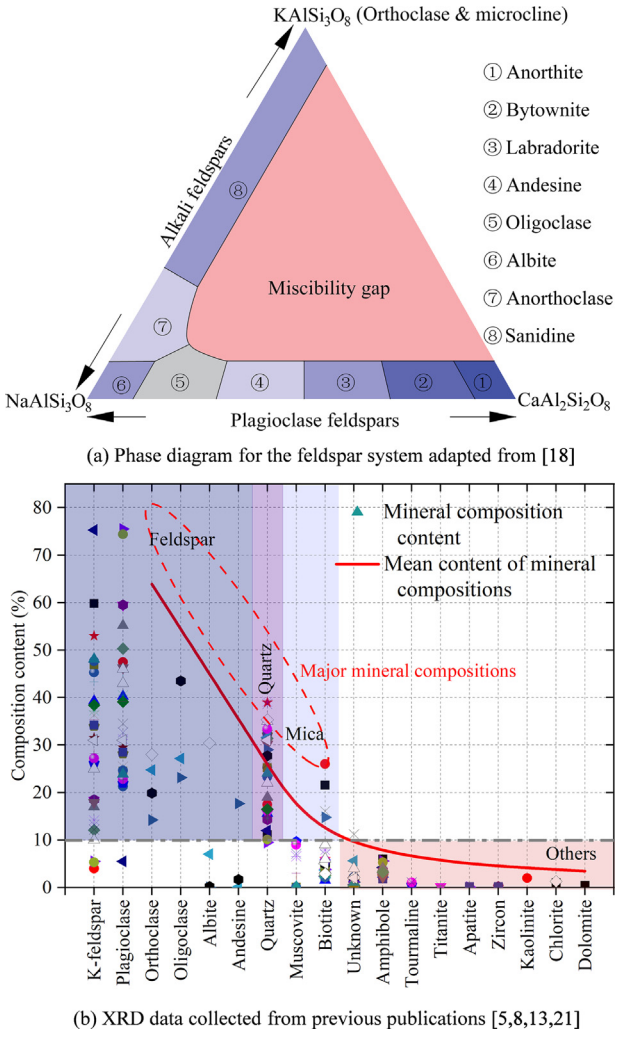

Fig. 1. Mineral composition contents in various granite samples: (a) Phase diagram for the feldspar system adapted from (Tuttle and Bowen, 1958 [18]); (b) XRD data collected from previous publications [5,8,13,21].

mineral phases that can form in this system as a function of temperature, pressure, and chemical composition [18]. For example, at atmospheric pressure, the feldspar system consists of three primary solid solutions: albite ($NaAlSi_3O_8$)-anorthite ($CaAl_2Si_2O_8$), albite-orthoclase ($KAlSi_3O_8$), and orthoclase-anorthite [19]. The diagram illustrates the different chemical components, such as potassium, sodium, and calcium, present in various types of feldspar [20]. Thus, the feldspar group encompasses several distinct types, including potassium feldspar, plagioclase, orthoclase, oligoclase, albite, andesine, etc.

The XRD technique can determine the mineral composition of granite. Fig. 1b presents the XRD data collected from previous publications, which are included in the body of the papers. The solid red line indicates the mean composition content of different mineral components, such as feldspar, quartz, mica, and other minerals. Feldspar, quartz, and mica ratios typically exceed 10%, thereby permitting them to be considered as the major mineral components within the granite.

This study grouped a variety of feldspars, depicted in Fig. 1a, as "feldspar" because of the similarity in their crystal structure and physical properties, regardless of their different chemical compositions. Likewise, this study categorized muscovite and biotite together under the classification of mica due to their similar crystal structures and chemical compositions [20]. As a result, this study

has focused on investigating the three primary components of granite: feldspar, quartz, and mica.

Fig. 2 is the histogram depicting the frequency distributions of physicomechanical properties and major component contents of granite based on research completed by previous scholars. The typical contents of quartz, feldspar, and mica in granite are 30%, 60%, and 10%, respectively. Additionally, granites have a typical density (ρ) of 2700 kg/m^3, void ratio of 0.8%, P-wave velocity (v_p) of 5500 m/s, UCS of 135 MPa, E of 40 GPa, and σ_t of 8 MPa.

2.2. Relationship between mineral composition contents and mechanical properties of granite

Fig. 3a presents the individual analysis of data from various publications that have described the relationship between the mineral composition contents and mechanical properties of granite. The red regions show a positive correlation, the blue regions represent a negative correlation, and the white regions indicate the absence of data. It is evident that the effect of mineral compositions on the mechanical properties of granites is subject to disagreement among researchers. For instance, most researchers found a positive correlation between quartz contents and UCS, σ_t, and E, while others proposed a negative correlation. This disparity in conclusions could be attributed to the relatively small sample sizes of the experimental datasets. Another possible cause is that the mechanical property of granite is independent of its mineral compositions.

This study summarized the data from additional publications, comprising 284 datasets for UCS, 149 for σ_t, and 110 for E. This study also computed the correlation values between various properties. Fig. 3b presents the results in a heatmap. The heatmap indicates that neither quartz nor feldspar negatively impacts the mechanical properties of granites, while mica does. The effect of quartz on E is more considerable (0.24), whereas the effect of feldspar on σ_t is also significant (0.17). Feldspar has minimal effect on E. The correlation values between mica content and UCS, E, and σ_t are −0.16, −0.26, and −0.28, respectively.

Nevertheless, one cannot simply establish a correlation between mineral compositions and mechanical properties of granite from the current database of publications. It is also likely that a limited database prevents the achievement of more precise results.

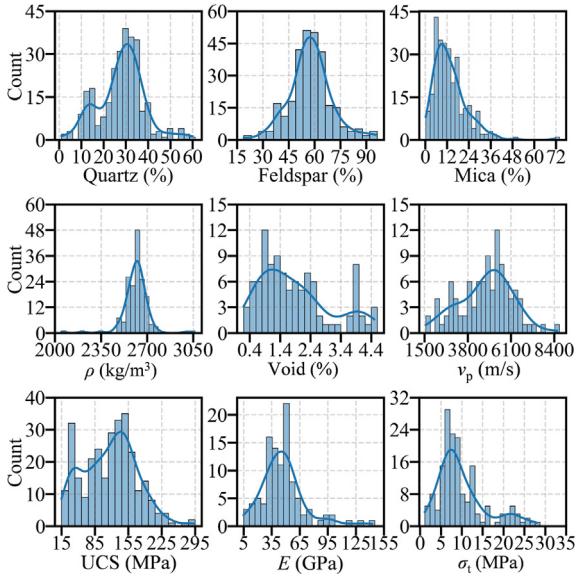

Fig. 2. Histogram regarding the major component contents and physicomechanical properties of granite [3–6,8,11,22–34].

Refs	Number of datasets	Quartz (%)			Feldspar (%)			Mica (%)		
		UCS	σ_t	E	UCS	σ_t	E	UCS	σ_t	E
[5]	8	−	−	−	+	+	+	−	−	−
[6]	12	−	−		−	+		+	−	
[8]	19	+	+	+	−	−	−	−	−	−
[22]	13	−			+			−		
[23]	6	−	−		−	−				
[25]	9	−			+			−		
[26]	17	+		+	+		+	+		+
[27]	9	+			+			−		
[28]	10	+			−					
[29]	10	+	−		−	+				
[30]	10	+	+		−	−		−	−	
[31]	15	+	+		−	−		−	+	
[32]	9	−	−		−	−		−	−	
[33]	9	+	+		−	−		−	+	
[34]	8	+	+		−	−		−	−	

(a) Individual analysis of data from references

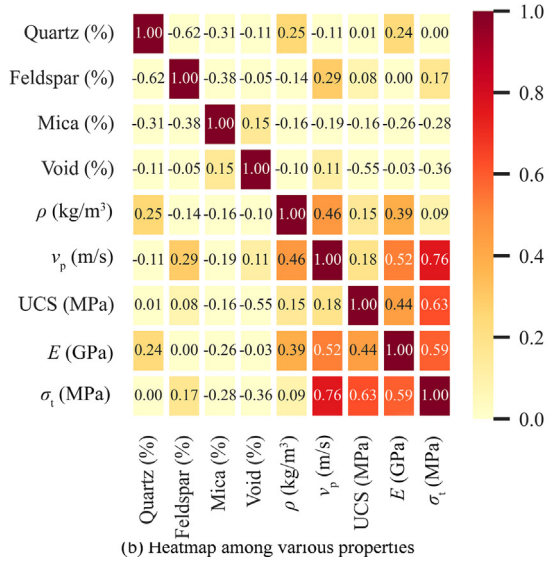

(b) Heatmap among various properties

Fig. 3. Relationship among mineral composition contents and mechanical properties [5–6,8,22,23,25–34].

The subsequent sections will use 351 PFC2D granite models with varying contents of major mineral compositions to simulate the UCS and DTS tests, resulting in a definitive conclusion.

3. Numerical simulation using PFC2D

3.1. DIP technique on the granite specimen

Granite is an intrusive igneous rock made of minerals visible to the naked eye [35,36], such as mica in the darkest color, quartz in the medium color, and feldspar in the lightest color [37]. Fig. 4a is the digital image of a granite sample with a diameter of 50 mm and a height of 100 mm from Li et al. [37]. The granite specimen contains three major components (59.7% feldspar, 31.4% quartz, and 8.9% mica). The digital image consists of pixel matrices composed of three channels, namely red, green, and blue (RGB), as illustrated in Fig. 4c. By employing the DIP method, it is feasible to distinguish between the distinct mineral compositions of granite from a two-dimensional (2D) perspective, assuming different minerals have different colors and the same minerals have identical colors. Typically, the quality of an image impacts the computational outcomes of the DIP technique [38]. Therefore, this study enhances the image quality to ensure it conforms to the requisite standards for image processing.

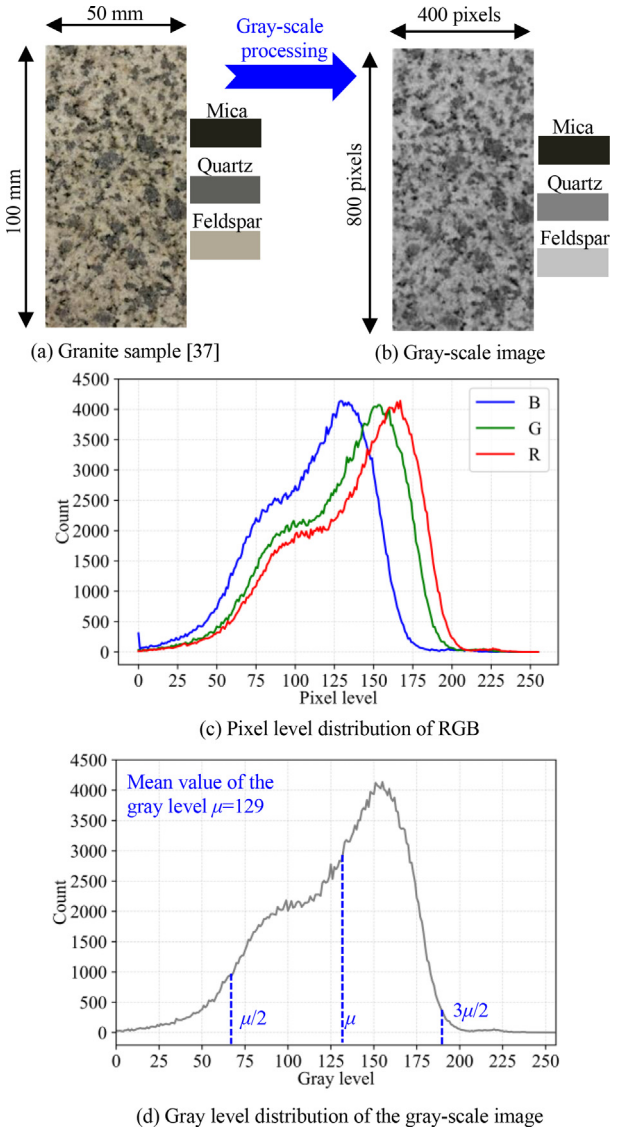

Fig. 4. Basic information on the granite sample image from [37].

Introducing the DIP technique in this study aims to appropriately determine the mineral compositions of granite without additional physical information and to use the results for numerical simulation modeling. In this study, however, a single channel of the gray-scale image satisfied the image recognition requirements and increased the efficiency of DIP by lowering the number of channels. Therefore, this process converted the digital image to gray-scale, as depicted in Fig. 4b. Fig. 4d illustrates the gray level distribution of the gray-scale image. The mean value of the gray level (μ) of the granite specimen is 129.

Fig. 5b depicts a selected region from Fig. 5a. Fig. 5c is the gray level of the selected 15×15 pixels region, with values between 0 and 255. The gray level represents the brightness of the pixel, e.g., mica should have the lowest brightness, while feldspar should have the highest. By dividing the gray-scale values into three intervals, it is capable of distinguishing between the three major mineral components in the granite specimen, known as threshold segmentation. This work introduces two methods of threshold segmentation: the mean value-based DIP method and the XRD-based DIP method (Fig. 5d and e).

Fig. 5d suggests the mechanism of the mean value-based DIP method. It indicates that when the exact composition contents of the granite sample were unknown, the value of μ would be utilized as the initial threshold value. Next, Fig. 4d shows the determination of various initial segmentation intervals as 0–μ/2, μ/2–μ, μ–3μ/2, and 3μ/2–255. However, to better match the original gray-scale image, the threshold value required continuous adjustment based on the initial threshold value. This study, for instance, only considered three major components of granite: feldspar (highest gray level), quartz (medium gray level), and mica (lowest gray level). Also, as shown in Fig. 5c, most pixels have gray levels of less than 200. Hence, this study merged the intervals of μ–3μ/2 and 3μ/2–255. By continuous adjustment, the initial segmentation intervals were ultimately altered to 0–μ/2: 0–65 (mica), μ/2–μ: 65–129 (quartz), and μ–255: 129–255 (feldspar). The mean value-based DIP methodology determined that the mineral component contents of feldspar, quartz, and mica were 56.7%, 38.6%, and 4.7%. Notably, these values are relatively similar to the exact XRD data of 59.7%, 31.4%, and 8.9%, respectively.

Table 1 illustrates the mean value-based DIP method outcomes for additional granite samples from additional publications [13,39]. The contents of some mineral compositions in granite computed by the mean value-based DIP method were similar to the exact XRD data, whereas others contained some errors. For example, applying the mean value-based DIP method to the granite sample analyzed by Zhang et al. [13], it reveals a biotite content of 6.21%, which closely approximates the exact value of 6.00%. Conversely, other mineral components displayed significant errors. In comparison, the mean value-based DIP method applied to the granite sample studied by Yang et al. [39] demonstrated lower errors than those observed in the analysis of the granite sample investigated by Zhang et al. [13]. In reality, it is not feasible to ascertain the exact mineral composition of granite solely based on its surface characteristics. Notwithstanding, the mean value method retains its practical utility, as it allows for the estimation of specific mineral fractions in rock samples where XRD tests were not performed. Moreover, the data acquired using the mean value method may be entered into numerical simulation software to facilitate model reconstruction, thereby adding to its overall reference value.

The XRD-based DIP method involved the exact composition contents of the granite sample under examination. In this study, the granite sample depicted in Fig. 5a consisted of 8.9% mica, 31.4% quartz, and 59.7% feldspar. As the total number of pixels in the granite image amounted to 320000 pixels, this study calculated the cumulative pixel numbers corresponding to values below a certain gray level A using Fig. 4d. Specifically, 8.9% of the pixels, i.e., 28480 pixels, should have gray levels between 0 and A, which was found to be 80. Similarly, this study determined segmentation value for quartz and feldspar was 126. Ultimately, this study segmented the intervals as (0, 80), (80, 126), and (126, 255). Meanwhile, in this case, the similarities of the results of two threshold segmentation methods demonstrated that the mean value-based DIP method was acceptable to some extent when the exact composition contents were unknown.

Therefore, the utilization of the DIP technique allows for the restoration of the mineral composition content and spatial distribution of the granite sample. Subsequently, based on the results of the DIP technique, a numerical model that adheres to the mineral composition content and spatial distribution of the actual granite sample is established, which represents an effective approach to calibrating the numerical model.

3.2. Numerical model establishment

This research used the discrete element method PFC2D, comprised of discrete particles that move independently and interact

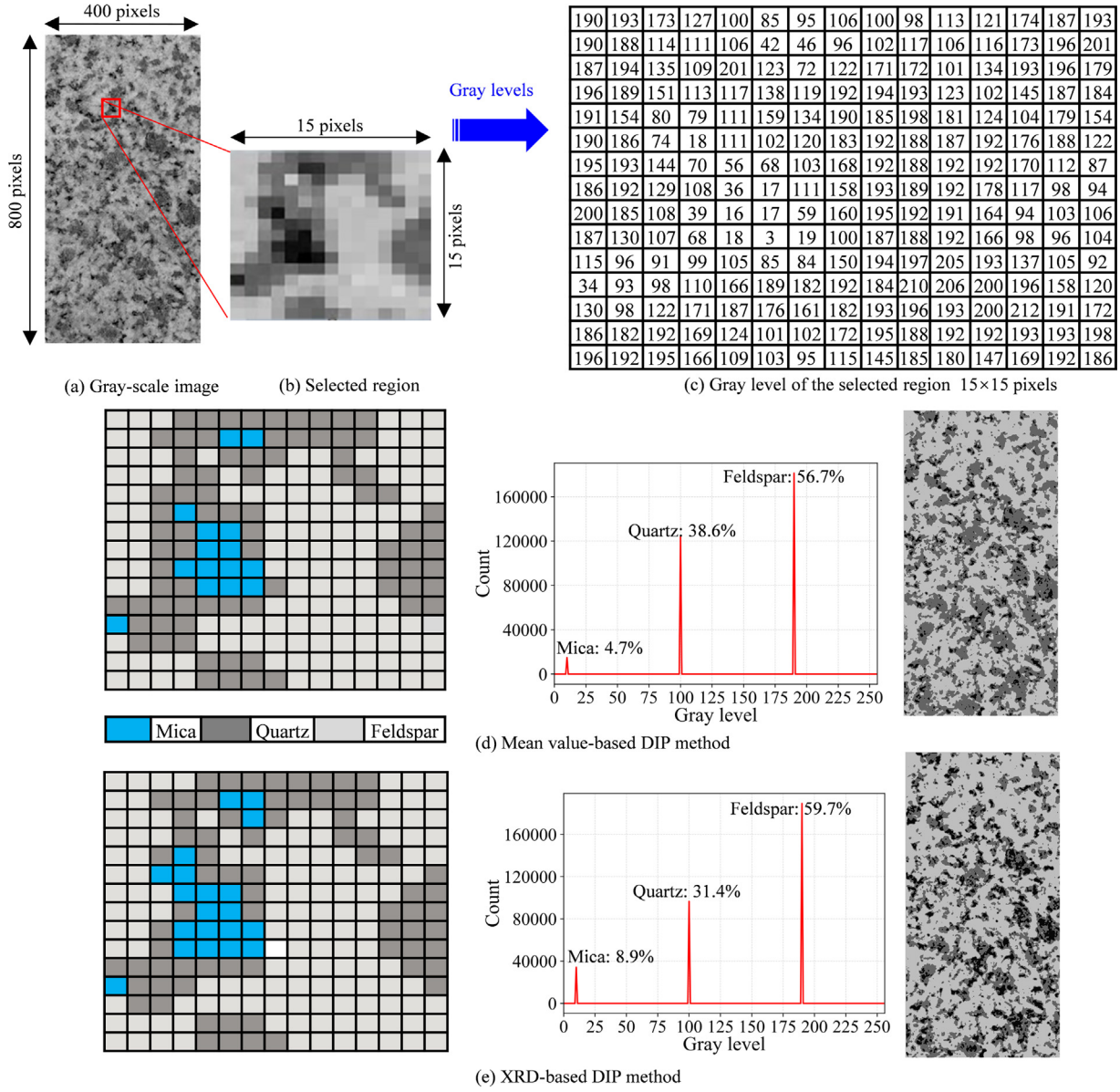

Fig. 5. Two threshold segmentation methods of DIP to detect major components in the granite specimen.

Table 1
Mean value-based DIP method executed on other granites.

Granite images	XRD data	DIP results	Components (DIP)	Error
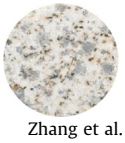 Zhang et al. [13]	Feldspar: 53.00% Biotite: 6.00% Quartz: 39.00% Others: 2.00%	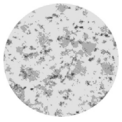	Feldspar: 71.98% Biotite: 6.21% Quartz: 21.69% Others: 0.76%	35.81% 3.50% 44.40% 62.00%
 Yang et al. [39]	Feldspar: 59.85% Biotite: 21.56% Quartz: 11.12% Others: 7.47%	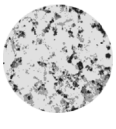	Feldspar: 66.10% Biotite: 21.75% Quartz: 7.64% Others: 4.50%	10.40% 0.89% 31.30% 39.76%

during pair-wise encounters. By allowing particles to bond at their points of contact, it is possible to depict more complex behavior. Upon reaching the strength limit, the bond breaks, allowing tensile forces to arise between particles. This makes it possible for tensile forces to develop between particles. The method can then model the interaction between these bonded "blocks", including the formation of fissures that may lead to the fragmentation of blocks into smaller blocks.

This study used the XRD-based DIP method to determine the component spatial distribution data of granite, as illustrated in Fig. 6b, for establishing the PFC2D model. This study obtained the component spatial distribution data by determining the coordinates and gray levels of each pixel, then imported it into PFC2D to identify the grain boundaries of different components. Subsequently, generating balls with varying sizes inside the grain boundary. Previous studies have utilized PFC2D to simulate granite particles with minimum sizes ranging from 0.1 [37], 0.15 [40], 0.4 [16], and 0.5 mm [13], among others. In this study, particle sizes ranged from 0.16 to 0.3 mm, consistent with current research findings. The total number of particles in the established numerical model is 33100.

3.3. Contact models in PFC2D

The PFC2D model [41] typically employs various contact models, namely, the linear contact bond model (CBM), linear parallel bond model (PBM), flat-joint model (FJM), and smooth joint model (SJM), for microparticles of granite. CBM involves a contact bond with constant normal and shear stiffnesses, lacking relative rotation resistance, and allowing resistance to tension and shear until the bond strength is exceeded. However, CBM model lacks radius, shear, and normal stiffness and cannot resist a bending moment [42]. PBM, on the other hand, entails relative motion at the contact following parallel bond generation, leading to the development of force and moment within the bond material. Nonetheless, PBM exhibits drawbacks such as suboptimal compression-tension ratio, the inability of spherical particles and parallel linkages to provide sufficient rotational resistance, and diminutive internal friction angle of the model [42]. FJM, in turn, involves the installation of contact bonds between particles with a small installation gap, enabling the simulation of interface behavior between two artificial surfaces firmly linked to body components. Meanwhile, SJM simulates the behavior of a smooth interface generated by a joint plane. It primarily encapsulates the impact of joint orientation and inclination on the joint, which in turn significantly influences the behavior of the entire rock mass. However, it should be noted that SJM does not take into account the local particle contact geometry surrounding the joint plane [43].

Previous studies have widely utilized the PBM to examine the microscopic failure process of different rocks under varying stress conditions [44]. Hence, it is suitable to adopt PBM in modeling the mechanical properties of granite samples in compression and tension tests conducted in this research due to the compact internal structure of granite, with few pores and a limited number of internal joint distributions.

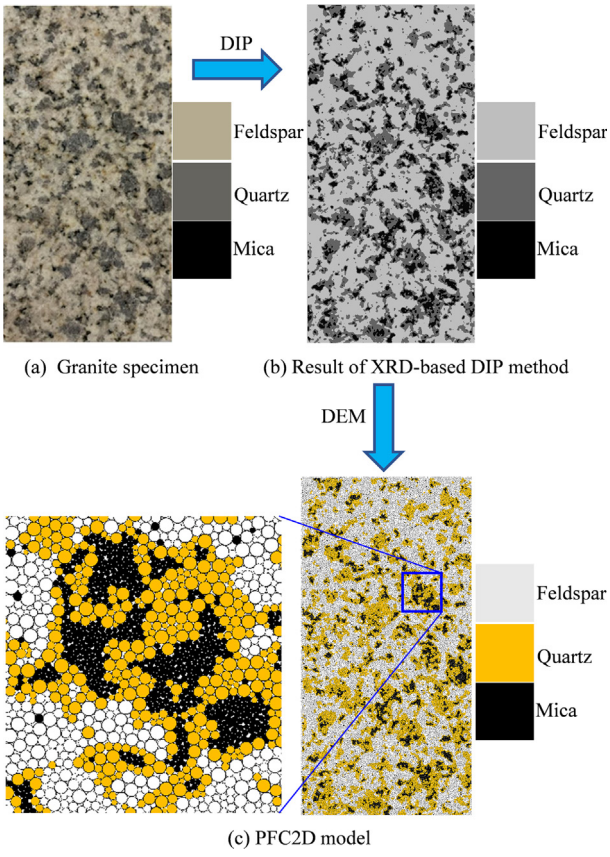

Fig. 6. PFC2D model based on the digital image of granite.

3.4. Micro-properties of the PFC2D model

The primary parameters for the PBM include the effective modulus (Emod), bond effective modulus (PB_Emod), normal-to-shear stiffness ratio (Kratio), bond normal-to-shear stiffness ratio (PB_Kratio), friction coefficient (Fric), particle density, tensile strength (PB_ten), cohesion (PB_coh), and friction angle (PB_fa). Fig. 7 illustrates the probability density distribution of multiple microscopic property parameters.

In order to calibrate the DEM parameters for granite, it is necessary to adjust its microscopic numerical parameters to fit the mechanical properties of the material during the calibration process. Therefore, this calibration requires continuous correction of the microscopic numerical parameters of granite. To facilitate the calibration process and achieve optimal results, it is important to establish initial value ranges for each microscopic parameter, which one can determine based on the results presented in Fig. 7.

This study selected the values corresponding to the 80% probability density peak of each parameter as the starting and ending values for the parameter range, as shown in Fig. 7. For instance, when establishing the range of Young's modulus (Emod) for each major component, the 80% density peak corresponds to the values of 15 and 60 GPa for feldspar, 25 and 75 GPa for quartz, and 10 and 45 GPa for mica. Consequently, the Emod value ranges for feldspar, quartz, and mica will be 15–60, 25–75, and 10–45 GPa, respec-

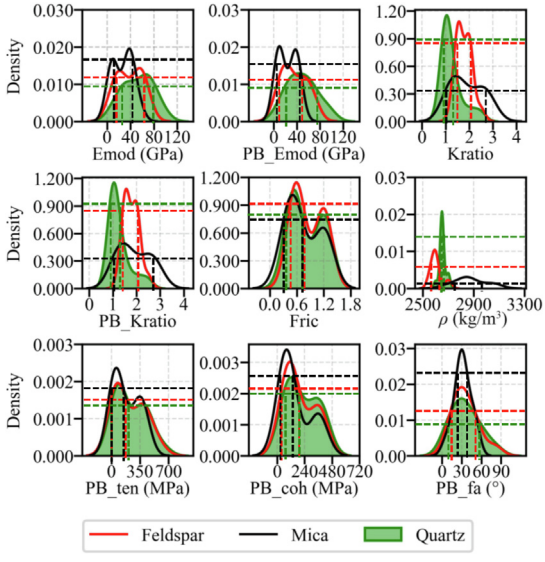

Fig. 7. Probability density function curves of microscopic property parameters of several mineral components in granite employed in PBM [3,11,12,15,16,37,45,46].

Table 2
Summaries of numerical parameter value ranges employed in PBM.

Properties	Feldspar	Quartz	Mica
Emod (GPa)	15–60	25–75	10–45
PB_Emod (GPa)	15–50	25–75	10–45
Kratio	1.7–2.2	0.8–1.4	1.0–2.6
PB_Kratio	1.7–2.2	0.8–1.4	1.2–2.0
Fric	0.4–0.8	0.4–0.8	0.4–0.7
ρ (kg/m^3)	2500–2700	2600–2700	2700–2900
PB_ten (MPa)	40–150	40–150	20–150
PB_coh (MPa)	30–180	30–180	20–150
PB_fa (°)	20–42	20–50	20–40

tively. Table 2 shows the ultimate numerical parameter value ranges utilized by the PBM. However, the summary of parameter value ranges provided in Table 2 can only serve as a reference for calibrating the numerical simulation. Additional parameter calibration adjustments within the range of values provided in Table 2 may be made if necessary.

3.5. Calibration of the PFC2D model

This section describes the calibration of the PFC2D model using experimental data (UCS) from a previous study [37]. Table 3 lists the parameter values of PBM employed in the PFC2D model. The parameters between two distinct minerals are the average of the parameters of each individual mineral [37]. Moreover, the current section undertakes a comparative analysis of the influence of diverse loading rates and boundary conditions on the UCS test outcomes. Fig. 8a illustrates the single-end loading executed at a rate of 0.1 m/s. Furthermore, Fig. 8b exhibits the utilization of loading rates of 0.1, 0.2, 0.4, and 0.8 m/s for both-ends loading. Fig. 8c–e present the UCS curves and failure modes of the granite specimen, encompassing both the numerical and experimental results.

Table 3
Parameter values of PBM employed in the PFC2D model.

Properties	Feldspar	Quartz	Mica	F-Q	F-M	Q-M
Emod (GPa)	18	28	10			
PB_Emod (GPa)	18	28	10	23	14	19
Kratio	2.2	1.4	2.0			
PB_Kratio	2.2	1.4	2.0	1.8	2.1	1.7
Fric	0.577	0.577	0.577	0.577	0.577	0.577
ρ (kg/m^3)	2500	2600	2700			
PB_ten (MPa)	42	48	22	45	32	35
PB_coh (MPa)	44	48	22	46	33	35
PB_fa (°)	40	30	40	35	40	35

Notes: F-Q is the interface between feldspar and quartz; F-M the interface between feldspar and mica; and Q-M the interface between quartz and mica.

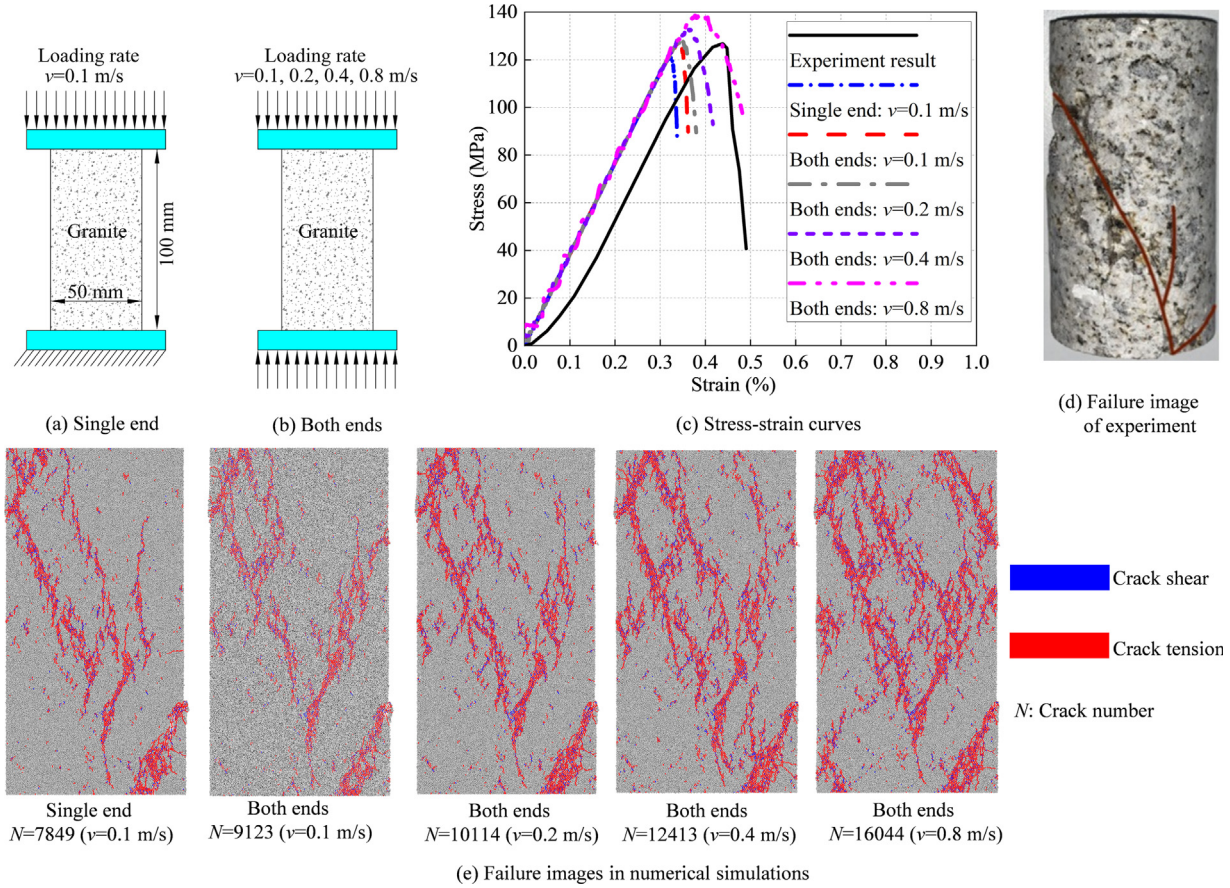

Fig. 8. UCS curves and the failure mode [37] under various loading patterns.

Various loading patterns, such as the loading rate and boundary condition, exert disparate impacts on the UCS and the failure mode, although the computed elastic modulus remains similar. A higher loading rate permits the granite specimen to enter the failure phase earlier, thereby shortening the computation time. However, it may result in overestimating the UCS and extending the scope of failure. This investigation has revealed that the UCS of granite obtained from numerical simulations agrees more closely with experimental results when applying loading rates of 0.1 and 0.2 m/s to both granite ends. Nevertheless, the fracture propagation pattern corresponding to a loading rate of 0.1 m/s is the closest to the actual damage mode. Conversely, the results obtained for a loading rate of 0.2 m/s do not correspond with the actual damage pattern due to the broader fracture propagation area. Consequently, this study selected the loading rate of 0.1 m/s for both ends of the PFC2D models and used the microscopic parameters presented in Table 3.

3.6. PFC2D models for analyzing mechanical properties of granites with varying major mineral contents under UCS and DTS tests

This section discusses granite samples with varying proportions of major components (quartz, feldspar, and mica), following the calibration and confirmation of the microscopic parameters of the PFC2D model. Particles in the PFC2D model have ID numbers ranging from 1 to 33100, making it easy to categorize them randomly into three groups based on their ID numbers. Notably, the investigation only focuses on the impact of different material compositions, with no consideration given to mineral size or porosity. Therefore, this study investigated 351 sets of models by constructing numerical models with different proportions from 0% to 100% (at 4% intervals) of each major component, as shown in Fig. 9. UCS tests and DTS tests were conducted on the numerical models to collect the UCS, σ_t, ε_{fail_UCS}, ε_{fail_DTS}, N_{crack_UCS}, N_{crack_DTS}, and E.

4. Numerical simulation results

This section discusses the results obtained from the PFC2D models. Fig. 10 shows the relationship between mechanical properties (UCS and σ_t) and major mineral component contents of granite, normalizing the values of UCS and σ_t to the range of 0–50% for a better visualization. Fig. 10 illustrates that quartz and feldspar exhibit positive effects on UCS and σ_t, while mica shows negative effects on UCS and σ_t. It also reveals that both UCS and σ_t values are relatively low in a limited range of major component contents, including feldspar (0–40%), quartz (0–50%), and mica (60%–100%). When feldspar exceeds 40% or quartz exceeds 50%, UCS and σ_t change significantly. However, this study can only obtain partial results from Fig. 10, and the specific mechanism of the effects of mineral contents on the mechanical properties of granite will require additional analyses.

The further analyses in this study utilized the concept of confidence ellipses for 2D datasets, as described in previous literature [47]. In a normal distribution, there is a 68.2% probability that the actual mean value falls within 1σ, 95.4% within 2σ, and 99.7% within 3σ, as depicted in Fig. 11. For the confidence ellipse, the horizontal radius equals to $\sqrt{1+p}$, and the vertical radius is $\sqrt{1-p}$, where p is the Pearson correlation coefficient, and it is defined by:

$$p = \frac{\mathrm{cov}_{xy}}{\sigma_x \sigma_y} \tag{1}$$

where cov_{xy} is the covariance of variable x and y; σ_x the standard deviation of variable x; and σ_y the standard deviation of variable y. Therefore, a large Pearson correlation coefficient (p) implies a statistically significant difference between the horizontal and vertical radii, resulting in a narrow confidence ellipse, as shown in Fig. 11b, which suggests a strong correlation. Conversely, a low Pearson correlation coefficient (p) indicates a minimal difference

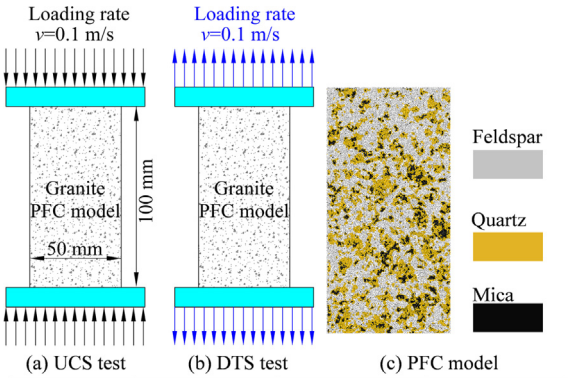

No.	Quartz (%)	Feldspar (%)	Mica (%)
1	0	0	100
2	4	0	96
3	8	0	92
⋮	⋮	⋮	⋮
349	0	12	88
350	0	8	92
351	0	4	96

(d) The setup of the mineral composition in PFC models

Fig. 9. PFC models of granite with various mineral component contents.

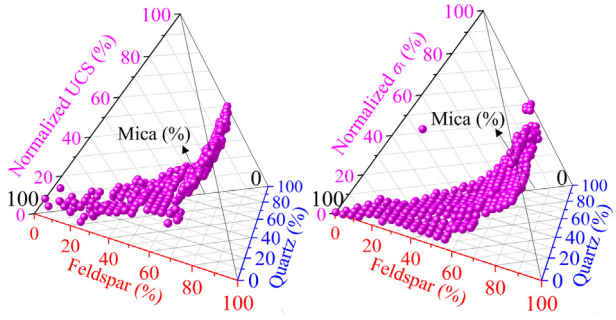

Fig. 10. Relationship between mechanical properties and major mineral component contents of granite.

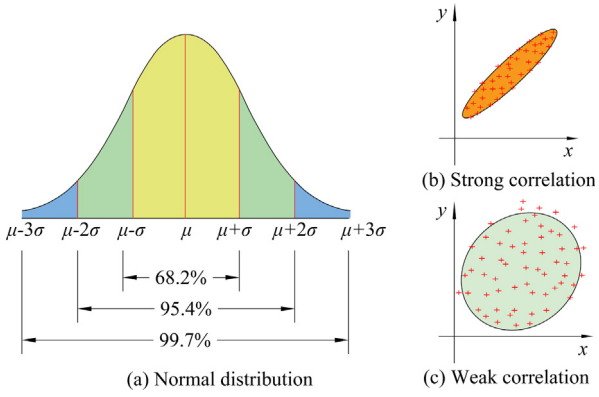

Fig. 11. Confidence interval of normal distribution and confidence ellipse.

between the horizontal and vertical radii, leading to a wide confidence ellipse, as shown in Fig. 11c, which represents a weak correlation.

4.1. Mechanical properties of granites with varying major mineral contents in the UCS test

Fig. 12 illustrates the correlations between the major mineral component contents of granites and their corresponding UCS, ε_{fail_UCS}, N_{crack_UCS}, and E, as determined via UCS tests. Consistent with previous findings (Fig. 3b), the results demonstrate that quartz and feldspar exert positive effects on UCS, while mica has a negative impact. Notably, mica exhibits the strongest correlation with UCS among the three major mineral components, with increasing mica content resulting in a significant decrease in UCS. In a particular mineral content range, such as 0–75%, the effect of quartz and feldspar contents on UCS is minimal. The magnitude of UCS is approximately 120 MPa; however, when the content

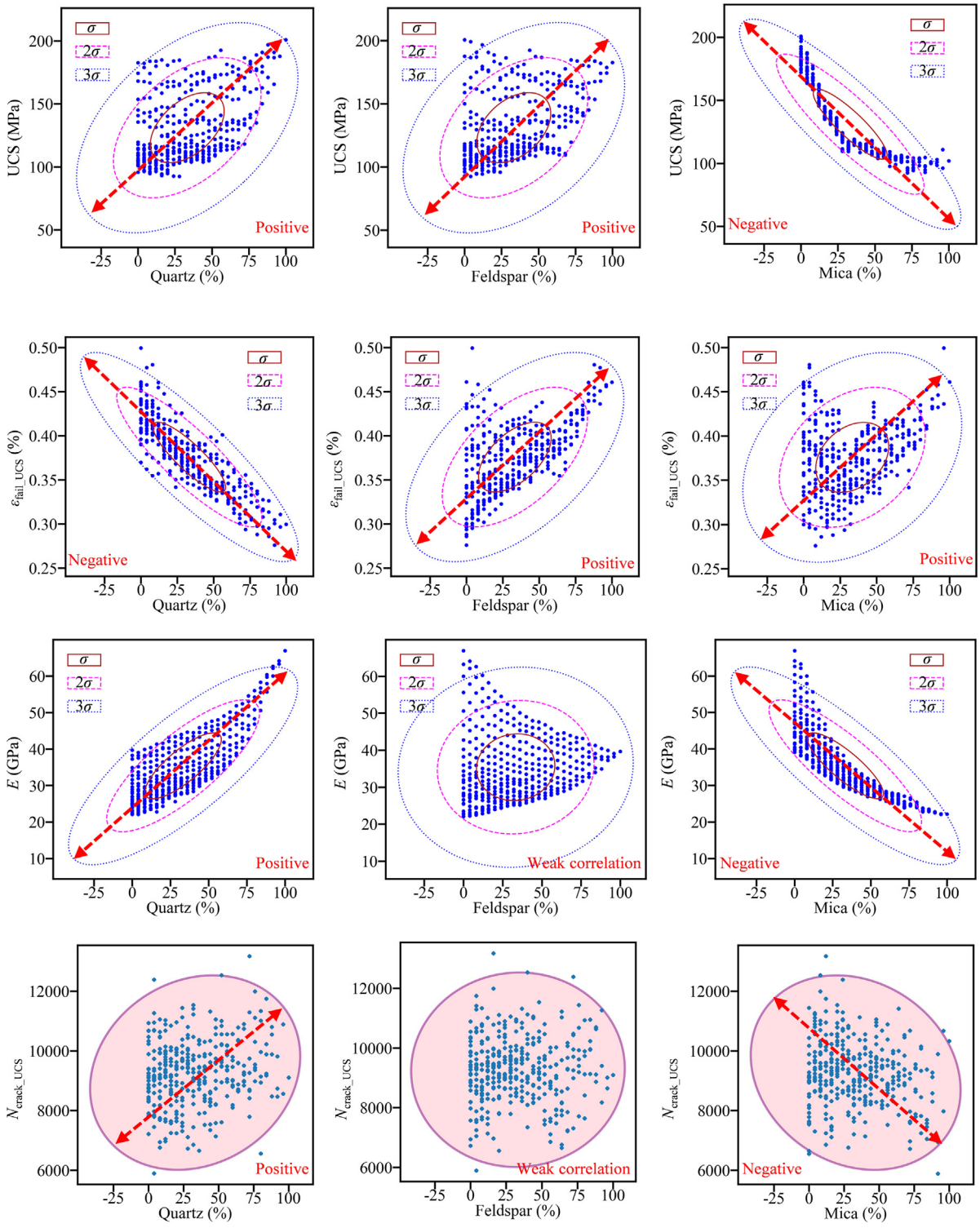

Fig. 12. Relationships between the major mineral compositions of granite and their corresponding UCS, ε_{fail_UCS}, N_{crack_UCS}, and E in the UCS test.

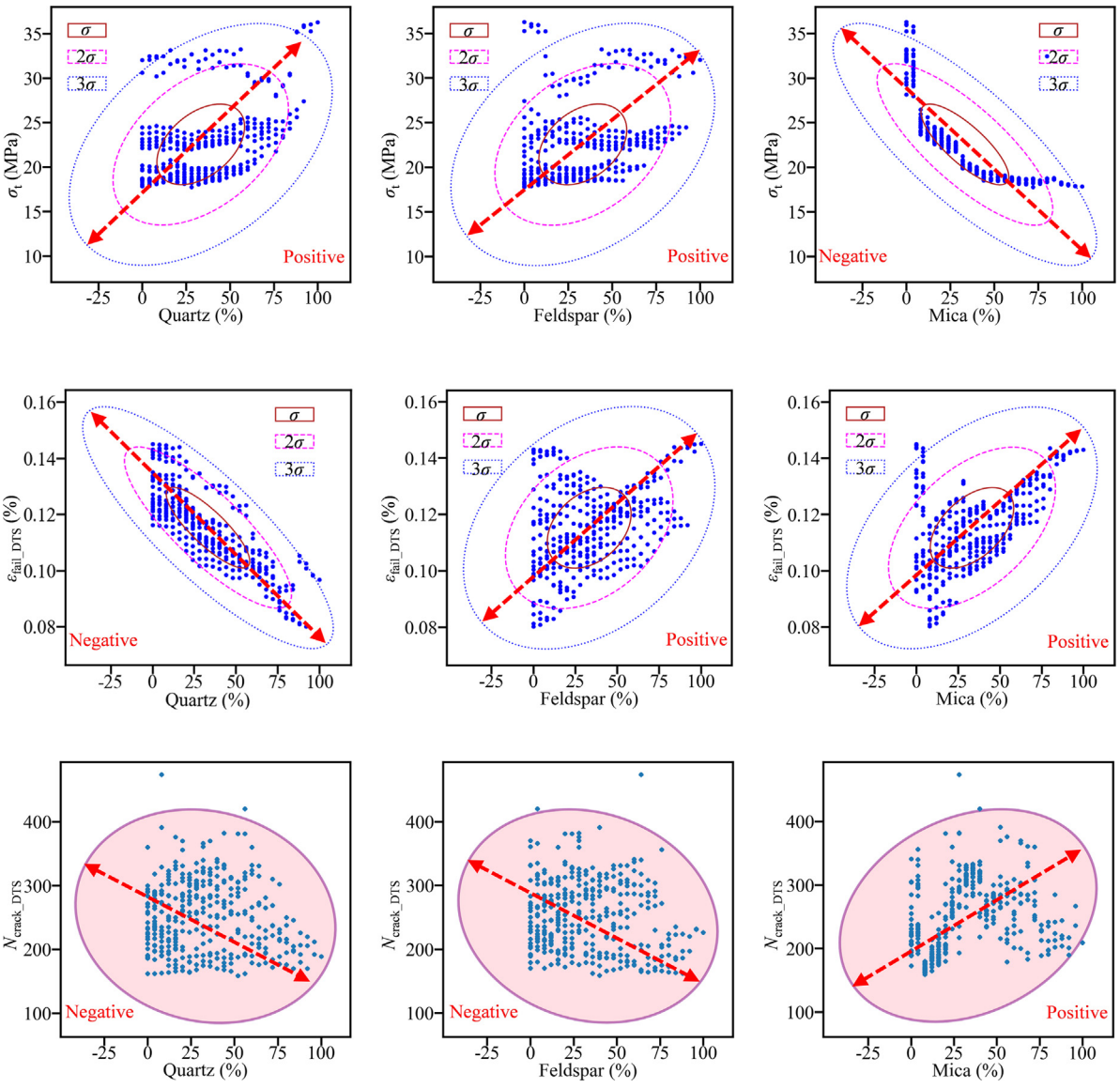

Fig. 13. Relationships between the major mineral compositions of granite and their corresponding σ_t, ε_{fail_DTS}, and N_{crack_DTS} in the DTS test.

exceeds 75%, UCS varies considerably and exhibits an increasing trend. Mica, however, has a very substantial effect on UCS when its content varies between 0 and 60%, as evidenced by a gradual decrease. When the mica percentage is greater than 60%, mica does not have a significant effect on the UCS.

The three major mineral components also show a correlation with failure strain. Quartz has a substantially higher correlation (negative correlation) with the failure strain than the other two components (positive correlation). This correlation suggests that the presence of quartz increases the brittleness of granite, whilst the presence of feldspar and mica increases its ductility. When the granite sample enters the failure phase, the number of microcracks will grow substantially. Therefore, a higher quartz content of granite may make it more susceptible to brittle failure in the UCS test. Additionally, the presence of feldspar and mica has positive effects on the failure strain, suggesting that they may contribute to the ductility of granite.

Quartz is found to have a significant impact on the elastic modulus, as most values fall within the range of 2σ of the confidence ellipse. However, the presence of mica has adverse effects. Feldspar has less effect on the elastic modulus of granite than quartz and mica. In addition, when the quartz content is within a particular range, such as 0 to 25%, the associated modulus is primarily centered around a certain value, i.e., 30 GPa. However, outside this range, the modulus increased gradually. The influence of mica on the elastic modulus ranges from 0 to 100%, meaning that as mica content increases, the modulus of elasticity decreases. The correlation between feldspar and elastic modulus is weak. Therefore, feldspar does not show a significant influence on the elastic modulus. The contents of three major mineral components have minor effects on the crack numbers in granite specimens. For example, an increase in quartz content is associated with a slight increase in crack numbers. In contrast, increased mica content exhibits a minor decrease in crack numbers. Nonetheless, feldspar content has a weak correlation with the crack number generated in the UCS test.

4.2. Mechanical properties of granites with varying major mineral contents in the DTS test

Fig. 13 shows relationships between the major mineral compositions of granites and their σ_t, ε_{fail_DTS}, and N_{crack_DTS} in the DTS

test. Similar to the findings of UCS tests, boosting the amount of quartz and feldspar strengthens granite in the DTS test, while increasing the proportion of mica has the opposite effect. Mica has the strongest correlation with the σ_t, followed by quartz and feldspar, meaning that the σ_t reduced significantly with increasing mica content. In a specific mineral content range, such as 0 to 80%, the effect of quartz and feldspar contents has a limited effect on σ_t, and σ_t is predominantly concentrated at roughly 20 MPa; however, when their amount reaches 80%, σ_t fluctuates much more and demonstrates a rising trend. Mica has a significant impact on σ_t when its concentration varies between 0 and 50%, as indicated by a progressive decline. When the proportion of mica exceeds 50%, the effect of increasing mica concentration on σ_t diminishes.

Similar to the results in the UCS test, there is an evident correlation between three major mineral components and the failure strain in the DTS test. Quartz has a substantial negative correlation with the failure strain in the DTS test. Mica and feldspar showcase a positive correlation with the failure strain in the DTS test. This correlation suggests that the presence of quartz increases the brittleness of granite, whilst the presence of mica and feldspar increases its ductility in the DTS test. When the granite sample enters the failure phase, the number of microcracks will grow substantially. Therefore, granite with higher quartz content may be more susceptible to brittle failure in the DTS test. Additionally, the presence of mica and feldspar has positive effects on the value of ε_{fail_DTS}, suggesting that they may contribute to the ductility of granite. In the DTS test, the influence of the three minerals in granite on the generation of fractures is rather limited. To illustrate, an escalation in the content of quartz and feldspar slightly reduces the production of fractures, whereas an increase in mica content slightly amplifies the number of fractures generated.

5. Discussion

Fig. 14 is the pair plot containing the properties mentioned above, which visualizes the qualitative relationships between the different variables. Fig. 15 shows the numerical results of the heatmap among various properties. This study found that the pattern exhibited by the numerical results was comparable to the calculated results shown in Fig. 3b. Specifically, this study found that

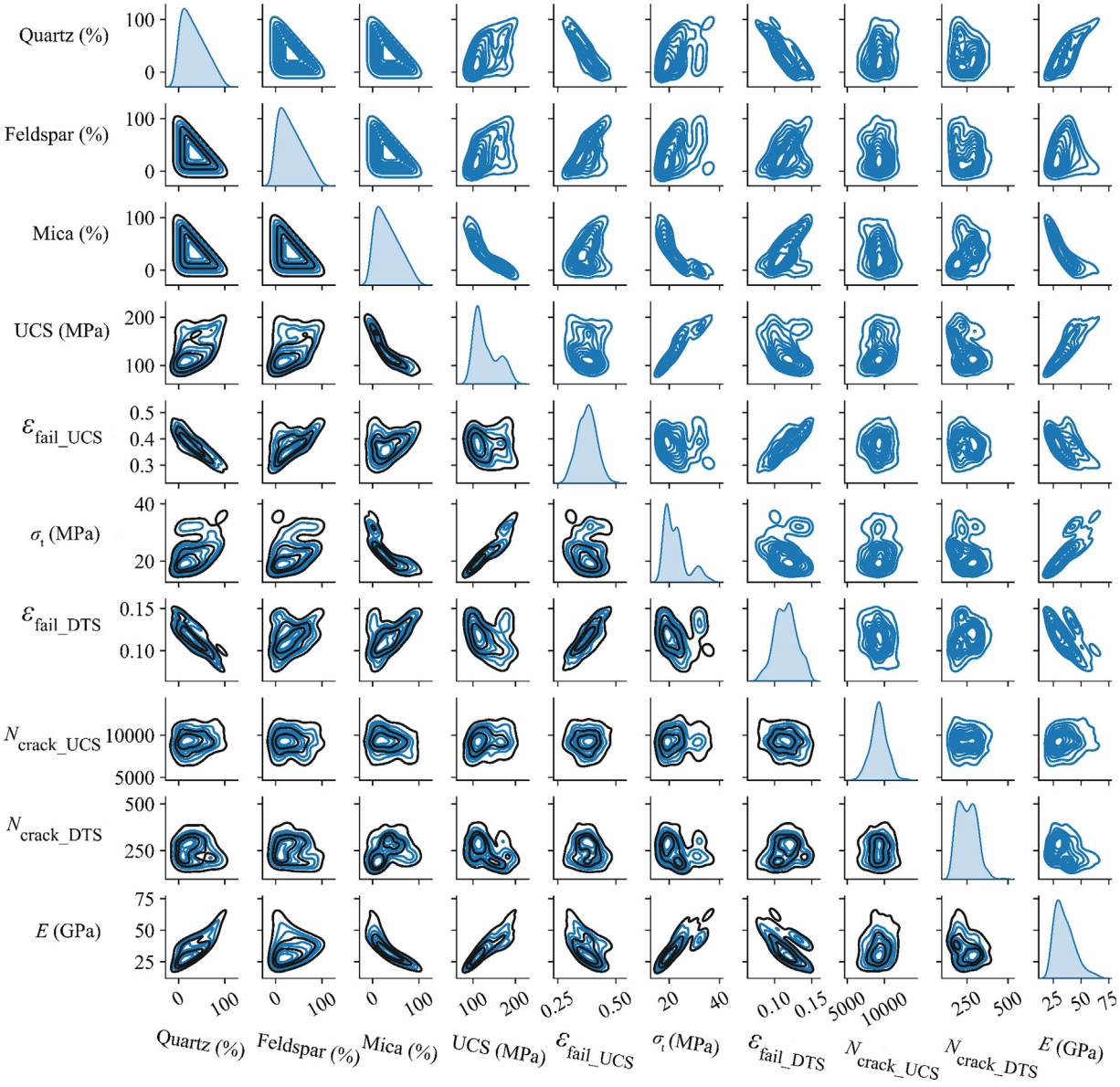

Fig. 14. Relationship between various properties of granite (numerical results).

there was no negative correlation between quartz and feldspar for UCS, σ_t, and E. Conversely, this study found mica to be negatively correlated with the UCS, σ_t, and E.

Table 4 displays the mechanical properties of quartz, feldspar, and mica. The compressive strength of mica is lower than that of quartz and feldspar, which implies that the strength of granite, including its UCS and σ_t, decreases as the content of mica increases. Conversely, the strength of granite increases as the contents of quartz and feldspar increase. Additionally, it has been observed that mica and feldspar possess a comparatively higher Poisson's ratio than quartz. This characteristic may potentially contribute towards enhancing energy dissipation, thereby alleviating stress concentration.

Based on an investigation of the crystal structure of three major mineral compositions, mica crystals consist of pseudo-hexagonal flakes, scales, plates, and occasional pseudo-hexagonal columns. Quartz crystals are hexagonal columns that are typically found in clusters, materials, and large aggregates. Feldspar crystals are predominantly in the form of plates or plate columns extending along a certain crystallographic axis. The crystal structures of mica and feldspar are more ductile than those of quartz, which permits their presence to raise the failure strain in granite [20]. These are potential causes for the low strength and high toughness of mica.

The trends observed in the numerical simulation outcomes align with the experimental results in terms of correlating various influential factors; however, it is important to highlight that the correlation coefficient values obtained differ. A potential explanation for this issue is that the granite samples used in the experiments come from different regions and are situated in different geological conditions. In addition to the differences in mineral fraction and distribution, there are also other differences, such as the degree of weathering of granite, the internal pores and natural fractures, and the grain size. The numerical simulations in this study concentrate exclusively on a single factor, mineral content, while neglecting other variables which might affect the mechanical properties of granite. For example, to investigate the influence of the mineral size of granite, it is essential to initially examine the mineral size characteristics of granite. From a statistical standpoint, the size of minerals in granite may adhere to a particular probability distribution, and the disparities in mechanical properties of granites corresponding to different size probability distributions are noteworthy. These aspects warrant further investigation in future research.

Therefore, the findings of this study are valuable because this research focuses on the qualitative influence of granite components on their mechanical properties. In engineering applications, it is occasionally necessary to predict the strength of granite based on several non-destructive parameters as inputs, such as XRD data, density, p-wave velocity, void ratio, etc. If one has a general understanding of the relationship between the inputs (non-destructive parameters) and the output parameter (strength), the prediction model can be optimized more effectively. Therefore, the outcomes of this study can provide a reference for analyzing the relationship between XRD data and the mechanical properties of granite.

However, the DIP technique used in this paper only processes 2D images, and the quality of 2D images is very demanding. The digital images used for DIP should ideally have even natural light on the rock surface. DIP is more suitable for distinguishing materials with large color contrasts, while it is difficult to identify materials with similar surface colors but vastly different properties. In order to significantly enhance the applicability of the DIP methodology, it is necessary to combine more feature extraction techniques in future studies. Meanwhile, it is crucial to expand the analysis to 3D, as this would provide a more accurate depiction of the stress distribution features of the rock sample under various stress conditions.

Overall, the findings of this study regarding the correlations between mineral components and mechanical properties of granite could have practical implications for engineering projects involving granite. For example, the information on which mineral components have positive or negative effects on UCS and failure strain could be useful in informing decisions about which types of granite to use for different applications. Similarly, the information on the effects of mineral content on elastic modulus could be useful in determining how to design structures made of granite to withstand different types of stresses. Meanwhile, the information on the relationships between mineral components and mechanical properties of granite could have broader implications for the understanding of geological processes. These findings may shed light on how different types of rock form and how tectonic processes affect them over time.

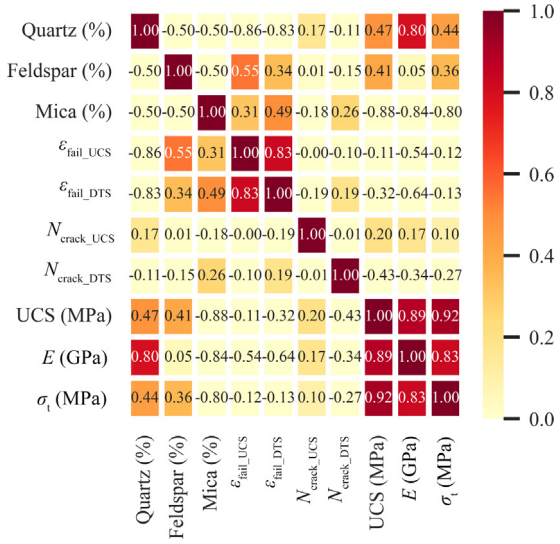

Fig. 15. Heatmap among various properties (numerical results).

Table 4
Lists of E and Poisson's ratio v of minerals.

Minerals	E (GPa) [48]	Compressive strength (MPa) [49]	v [48]
Quartz	95.6	100–300	0.079
Feldspar	69.7	100–300	0.301
Mica	88.1	70–140	0.248

6. Conclusions

This study initially used the DIP method to uncover both the contents and spatial distributions of minerals within the granite image. Subsequent to the DIP findings, PFC2D models with various mineral compositions (quartz, feldspar, and mica) were established to investigate the relationship between mineral composition and mechanical properties of granite. The results provide insights into the potential use of these methods in understanding the mechanical behavior of granite. As such, this study has drawn the following conclusions:

(1) The DIP method is effective in detecting the mineral composition contents and spatial distributions of granite samples. Studies can utilize the mean value-based DIP method if the exact mineral composition contents of the granite sample are unknown. If it is given, the XRD-based DIP method is capable of obtaining the mineral composition data (mineral

types and spatial distributions). By importing the computed mineral composition data into the numerical simulation software, one can accurately construct the discrete element model.

(2) Based on results computed by 351 sets of numerical models, the pattern exhibited by the numerical simulation is comparable to the literature data. There is no negative correlation between quartz and feldspar for UCS, σ_t, and E. A significant positive correlation exists between the quartz and E. However, the relationship between feldspar and E demonstrates a weak correlation. Mica has a significant negative correlation for UCS, σ_t, and E.

(3) The presence of quartz increases the brittleness of granite, whilst the presence of mica and feldspar increases its ductility in the UCS and DTS tests.

(4) Varying contents of major mineral compositions (quartz, feldspar, and mica) in granites have a minor influence on the number of cracks developed in UCS and DTS tests.

Acknowledgements

This research was financially supported by the Department of Mining Engineering at the University of Utah.

References

[1] Kumari WGP, Ranjith PG, Perera MSA, Chen BK, Abdulagatov IM. Temperature-dependent mechanical behaviour of Australian Strathbogie granite with different cooling treatments. Eng Geol 2017;229:31–44.
[2] Du K, Sun Yu, Zhou J, Khandelwal M, Gong FQ. Mineral composition and grain size effects on the fracture and acoustic emission (AE) characteristics of rocks under compressive and tensile stress. Rock Mech Rock Eng 2022;55(10):6445–74.
[3] Saadat M, Taheri A. A numerical approach to investigate the effects of rock texture on the damage and crack propagation of a pre-cracked granite. Comput Geotech 2019;111:89–111.
[4] Coggan JS, Stead D, Howe JH, Faulks CI. Mineralogical controls on the engineering behavior of hydrothermally altered granites under uniaxial compression. Eng Geol 2013;160:89–102.
[5] Sajid M, Coggan J, Arif M, Andersen J, Rollinson G. Petrographic features as an effective indicator for the variation in strength of granites. Eng Geol 2016;202:44–54.
[6] Yılmaz NG, Goktan RM, Kibici Y. Relations between some quantitative petrographic characteristics and mechanical strength properties of granitic building stones. Int J Rock Mech Min Sci 2011;48(3):506–13.
[7] Wang P, Yin TB, Li XB, Zhang SS, Bai L. Dynamic properties of thermally treated granite subjected to cyclic impact loading. Rock Mech Rock Eng 2019;52(4):991–1010.
[8] Tuğrul A, Zarif IH. Correlation of mineralogical and textural characteristics with engineering properties of selected granitic rocks from Turkey. Eng Geol 1999;51(4):303–17.
[9] Yesiloglu-Gultekin N, Sezer EA, Gokceoglu C, Bayhan H. An application of adaptive neuro fuzzy inference system for estimating the uniaxial compressive strength of certain granitic rocks from their mineral contents. Eng Geol 1999;51(4):303–17.
[10] Sun YT, Li GC, Zhang N, Chang QL, Xu JH, Zhang JF. Development of ensemble learning models to evaluate the strength of coal-grout materials. Int J Min Sci Technol 2021;31(2):153–62.
[11] Hofmann H, Babadagli T, Yoon JS, Zang A, Zimmermann G. A grain based modeling study of mineralogical factors affecting strength, elastic behavior and micro fracture development during compression tests in granites. Int J Min Sci Technol 2021;31(2):153–62.
[12] Peng J, Wong LNY, Teh CI. Influence of grain size on strength of polymineralic crystalline rock: New insights from DEM grain-based modeling. J Rock Mech Geotech Eng 2021;13(4):755–66.
[13] Zhang T, Yu LY, Wu BB, Tan YZ, Su HZ, Zhou LJ. Influence of grain-to-particle size ratio on the tensile mechanical response of granite based on a novel three-dimensional grain-based model. Eng Fract Mech 2022;259:108161.
[14] Hu XJ, Xie N, Zhu QZ, Chen L, Li PC. Modeling damage evolution in heterogeneous granite using digital image-based grain-based model. Rock Mech Rock Eng 2020;53:1–21.
[15] Wong LNY, Peng J, Teh CI. Numerical investigation of mineralogical composition effect on strength and micro-cracking behavior of crystalline rocks. J Nat Gas Sci Eng 2018;53:191–203.
[16] Yu LY, Zhang T, Wu DY, Wu BB, Ma LJ, Wei JB. Numerical investigation of the effect of grain size-to-particle size ratio on the dynamic fracture toughness of granite by using PFC3D-GBM. Geomech Geophys Geo Energy Geo Resour 2022;8:72.
[17] Granite, (n.d.). <https://nature.berkeley.edu/classes/eps2/wisc/granite.html> [accessed February 26, 2023].
[18] Tuttle OF, Bowen NL. Origin of granite in the light of experimental studies in the system $NaAlSi_3O_8$-$KAlSi_3O_8$-SiO_2-H_2O. In: GSA Memoirs. The Geological Society of America; 1958.
[19] Ghiorso MS, Sack RO. Chemical mass transfer in magmatic processes IV. A revised and internally consistent thermodynamic model for the interpolation and extrapolation of liquid-solid equilibria in magmatic systems at elevated temperatures and pressures. Contr Mineral and Petrol 1995;119(2-3):197–212.
[20] Howie RA, Zussman J, Deer WA. An introduction to the rock-forming minerals. London: Longman; 1992.
[21] Fourmeau M, Gomon D, Vacher R, Hokka M, Kane A, Kuokkala VT. Application of DIC technique for studies of Kuru granite rock under static and dynamic loading. Proc Mater Sci 2014;3:691–7.
[22] Přikryl R. Some microstructural aspects of strength variation in rocks. Int J Rock Mech Min Sci 2001;38(5):671–82.
[23] Buyuksagis IS. Effect of cutting mode on the sawability of granites using segmented circular diamond sawblade. Int J Rock Mech Min Sci 2001;38(5):671–82.
[24] Kobayashi M, Kuriki Y, Watanabe K, Chen YQ, Kusuda H, Mabuchi M. Microcrack growth patterns in Westerly granite specimens subjected to uniaxial cyclic loading. Int J JCRM 2010;5:103–10.
[25] Sousa LMO. The influence of the characteristics of quartz and mineral deterioration on the strength of granitic dimensional stones. Environ Earth Sci 2013;69(4):1333–46.
[26] Ündül Ö, Amann F, Aysal N, Plötze ML. Micro-textural effects on crack initiation and crack propagation of andesitic rocks. Eng Geol 2015;193:267–75.
[27] Ersoy H, Acar S. Influences of petrographic and textural properties on the strength of very strong granitic rocks. Environ Earth Sci 2016;75:1461.
[28] Sun Q, Zhang JS, Wang Z, Zhang H, Fang JY. Segment wear characteristics of diamond frame saw when cutting different granite types. Diam Relat Mater 2016;68:143–51.
[29] Yusof NQAM, Zabidi H. Correlation of mineralogical and textural characteristics with engineering properties of granitic rock from Hulu Langat, Selangor. Proc Chem 2016;19:975–80.
[30] Ajalloeian R, Jamshidi A, Khorasani R. Evaluating the effects of mineral grain size and mineralogical composition on the correlated equations between strength and schmidt hardness of granitic rocks. Geotech Geol Eng 2020. Article in press.
[31] Hemmati A, Ghafoori M, Moomivand H, Lashkaripour GR. The effect of mineralogy and textural characteristics on the strength of crystalline igneous rocks using image-based textural quantification. Eng Geol 2020;266:105467.
[32] Kahraman S, Canpolat AN, Fener M. The influence of microwave treatment on the compressive and tensile strength of igneous rocks. Int J Rock Mech Min Sci 2020;129:104303.
[33] Ahmed I, Basharat M, Sousa L, Mughal MS. Evaluation of building and dimension stone using physico-mechanical and petrographic properties: A case study from the Kohistan and Ladakh batholith, Northern Pakistan. Environ Earth Sci 2021;80:759.
[34] Jamshidi A. Predicting the strength of granitic stones after freeze-thaw cycles: Considering the petrographic characteristics and a new approach using petro-mechanical parameter. Rock Mech Rock Eng 2021;54(6):2829–41.
[35] Shi C, Yang WK, Yang JX, Chen X. Calibration of micro-scaled mechanical parameters of granite based on a bonded-particle model with 2D particle flow code. Granul Matter 2019;21:38.
[36] Tan X, Konietzky H, Chen W. Numerical simulation of heterogeneous rock using discrete element model based on digital image processing. Rock Mech Rock Eng 2016;49(12):4957–64.
[37] Li MY, Wu ZJ, Weng L, Liu QS, Chu ZF. Quantitative relationships between the mineral composition and macro mechanical behaviors of granite under different temperatures: Insights from mesostructure-based DEM investigations. Comput Geotech 2022;148:104838.
[38] Sun Q, Zheng J, Coop MR, Altuhafi FN. Minimum image quality for reliable optical characterizations of soil particle shapes. Comput Geotech 2019;114:103110.
[39] Yang SQ, Ranjith PG, Jing HW, Tian WL, Ju Y. An experimental investigation on thermal damage and failure mechanical behavior of granite after exposure to different high temperature treatments. Geothermics 2017;65:180–97.
[40] Saadat M, Taheri A. Modelling micro-cracking behaviour of granite during direct tensile test using cohesive GBM approach. Eng Fract Mech 2020;239:107297.
[41] Itasca Consulting Group, Inc. PFC — Particle Flow Code, version 7.0. Minneapolis: Itasca; 2021.
[42] Wu SC, Xu XL. A study of three intrinsic problems of the classic discrete element method using flat-joint model. Rock Mech Rock Eng 2016;49(5):1813–30.
[43] Huang D, Wang JF, Liu S. A comprehensive study on the smooth joint model in DEM simulation of jointed rock masses. Granul Matter 2015;17(6):775–91.
[44] Liakas S, O'Sullivan C, Saroglou C. Influence of heterogeneity on rock strength and stiffness using discrete element method and parallel bond model. J Rock Mech Geotech Eng 2017;9(4):575–84.

[45] Zhang XP, Ji PQ, Peng J, Wu SC, Zhang Q. A grain-based model considering pre-existing cracks for modelling mechanical properties of crystalline rock. Comput Geotech 2020;127:103776.
[46] Xu ZY, Li TB, Chen GQ, Ma CC, Qiu SL, Li Z. The grain-based model numerical simulation of unconfined compressive strength experiment under thermal-mechanical coupling effect. KSCE J Civ Eng 2018;22(8):2764–75.
[47] Schelp C. An alternative way to plot the covariance ellipse, carstenschelp. github Io; 2018. <https://carstenschelp.github.io/2018/09/14/Plot_Confidence_Ellipse_001.html> [accessed September 25, 2022].
[48] Bass JD. Mineral Physics & Crystallography: A Handbook of Physical Constants. AGU Reference Shelf. Washington: American Geophysical Union; 1995. p. 45–63.
[49] Deer WA, Howie RA, Zussman J. Rock-Forming Minerals Volume 1A: Orthosilicates. London: Geological Society of London; 1982.